Designing of Phase Advance of the Carrier Signals Using Intelligent Neural Networks

Zoran Stankovic[1], Ivan Milovanovic[2], Nebojsa Doncov[1], Maja Sarevska[3], Bratislav Milovanovic[2]
[1]Faculty of Electronic Engineering
University of Nis, A. Medvedeva 14
18000 Nis
{zoran.stankovic, nebojsa.doncov@elfak.ni.ac.rs}
[2]The Singidunum University
DLS center Nis
18000 Nis
{ivanshix@gmail.com, batam@pogled.net}
[3]European University - Republic of Macedonia (EURM)
{maja.sarevska@eurm.edu.mk}

ABSTRACT: *To measure the phase advance of the carrier signal using intelligent neural networks is proposed that used a new model. To achieve this task, we have developed the system based on multilayer perceptron network. In this process, to find the near value of ions concentration, we have used the latitude of the observed receiving terminal and the present point in time. The obtained data enable the measurement of the phase advance of the carrier signal. This is done with the propagation through the ionosphere. The present model design helps the measurement of ionospheric carrier phase advance and it is tested in the target areas.*

Keywords: EM Propagation, Ionosphere, Neural Networks, Neural Modelling

Received: 17 October 2020. Revised 14 January 2021. Accepted 27 January 2021

DOI: 10.6025/jic/2021/12/2/43-53

1. Introduction

The ionosphere is a layer of an atmosphere that contains a much higher concentration of free ions than other layers of the atmosphere. Because of this property, it represents such an electromagnetic environment that strongly influences the change in the characteristics of EM waves that pass through it [1-5]. If signals of wireless communication systems are viewed in one part of their path through the ionosphere (typical examples of the satellite communication system signals), then changes in the trajectory of the signal, changes in signal degradation, changes in the frequency of the signals, changes in the phase carrier, and changes In signal polarization [5]. These changes affect the proper operation of the aforementioned wireless systems, and the space-time characterization of these changes can be of great importance for their construction and exploitation. A typical example of the negative impact of signal changes in the ionosphere is the possibility of an error in determining the position of users on the ground using satellite navigation systems (such as the Global Positioning System - GPS) due to a change in signal degradation.

Changing the concentration of free electrons in the ionosphere dominates the change in the characteristics of the signal that extends through the ionosphere [1-5]. Therefore, the knowledge of the distribution of the electron concentration on the signal path propagation through the ionosphere is of vital importance for describing and modeling the change in the characteristics of the signal. The concentration of free electrons in the ionosphere as well as the distribution of this value at altitude (the elevation profile of the ionosphere) depends on a large number of spatial and temporal parameters, and the most important ones are: the geographical location of the site above which the profile of the ionosphere, the seasons, the time during the day and the intensity of the sun Activities within the 11-year-old Swabian cycle.

In order to describe the functional dependence of a certain signal parameter on the concentration of an electron in the ionosphere, the volume usually represents the amount that represents the total concentration of free electrons on the path of expansion through the ionosphere or shortened TEC (Total Electron Content) [1,5]. Determining the TEC values for the desired geographical locations and the desired weather moments is a rather complex task. One approach is the use of specialized software for modeling height profiles of the ionosphere [5,6]. These software are very expensive and are generally not publicly available. The second approach is to make TEC values read from various tables and complex graphs obtained by measurements on a limited set of geographic locations using interpolation for the desired geographic location [2,6]. This method is painstaking and often imprecise.

An alternative approach to determining the TEC value that can overcome some of the problems of the above-mentioned approaches is the modeling of the spatial-temporal dependence of TEC values using artificial neural networks [7- 10] as shown in [11]. There is a developed neuronal model for the prediction of additional time signal delay in the ionosphere for the winter and summer periods.

This paper is a continuation of the conducted research presented in [11]. Using the multilayer perceptron network (MLP) [7-11] which was trained to determine the TEC value during the autumn and spring period, developed a neuronal model for the Ionospheric Carrier Phase Advance.

2. Neural Model of the Ionospheric Carrier Phase Advance

Ionospheric Carrier Phase Advance can be calculated using the formula [5]

$$\Delta\phi = \frac{4.824 \cdot 10^{-5}}{f} \cdot TEC \qquad [^\circ] \qquad (1)$$

where *TEC* is the aforementioned electron density along the signal path from the transmitter to the receiver expressed in units of *electron/m*^{2}, and *f* is the carrier frequency is expressed in Hz. For the realization of the neural model, the dependence of the TEC value on the latitude and time of the day for the Mediterranean region obtained by the measurements in the autumn period during the mean solar activity and the solar flux of 110 (Figure 1) were taken and measurements in the spring period in low solar activity and solar Flux of 90 (Figure 2)

Architecture of the neural model of the ionospheric carrier phase advance over the Mediterranean area (MLP_PA – MLP *Phase Advance*) is presented in Figure 3. This model models the dependence of the ionospheric carrier phase advance on the geographic latitude value of the observed site in the Mediterranean region, *la*, the time of the day, *h*, and the signal frequency, *f*,

$$\Delta\phi = f_{MLP\_PA}(la, h, f) \qquad (2)$$

The MLP_PA model consists of MultiLayer Perceptron (MLP) network that models the dependence of TEC values on the geographic latitude values of the observed spot in the Mediterranean region and the time of the day

$$TEC = f_{MLP\_TEC}(la, h) \qquad (3)$$

and is designated in the model by the MLP_TEC block, and from the ionospheric carrier phase advance calculation block which calculates the ionospheric carrier phase advance calculation according to the equation (1) based on the estimated TEC value by the MLP_TEC network and the frequency values.

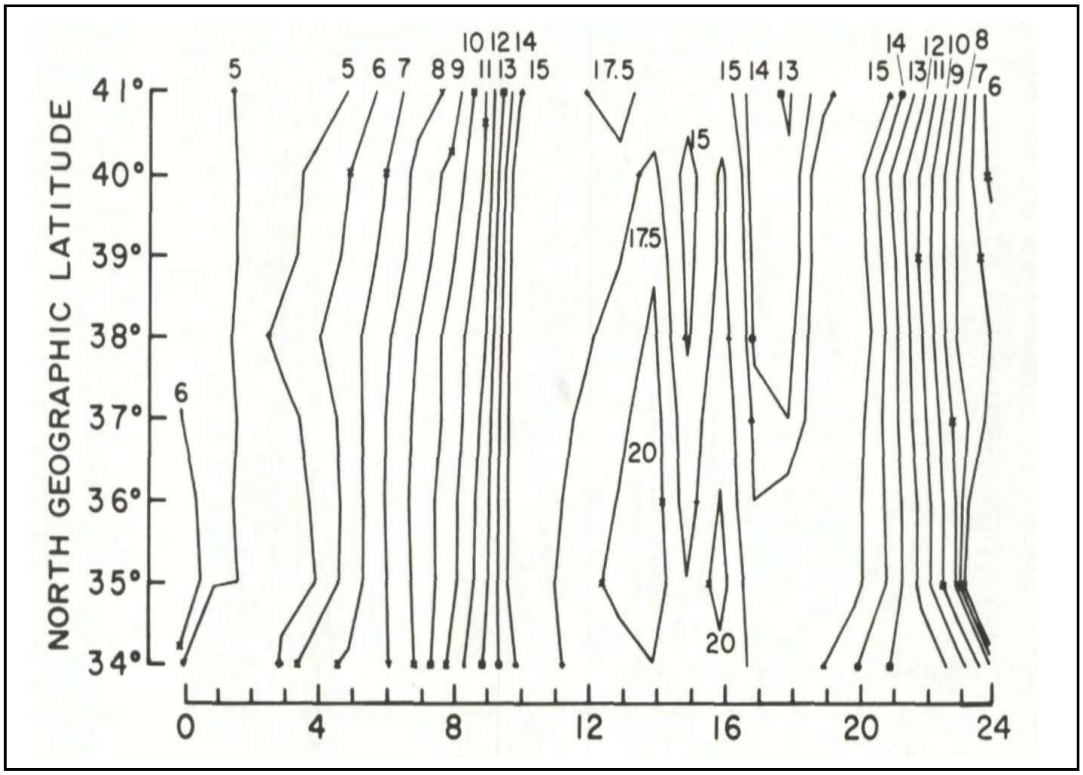

Figure 1. Contour plots of measured TEC data vs. hours and latitude for autumn (TEC units are in10^{16} elektron/ m^2)

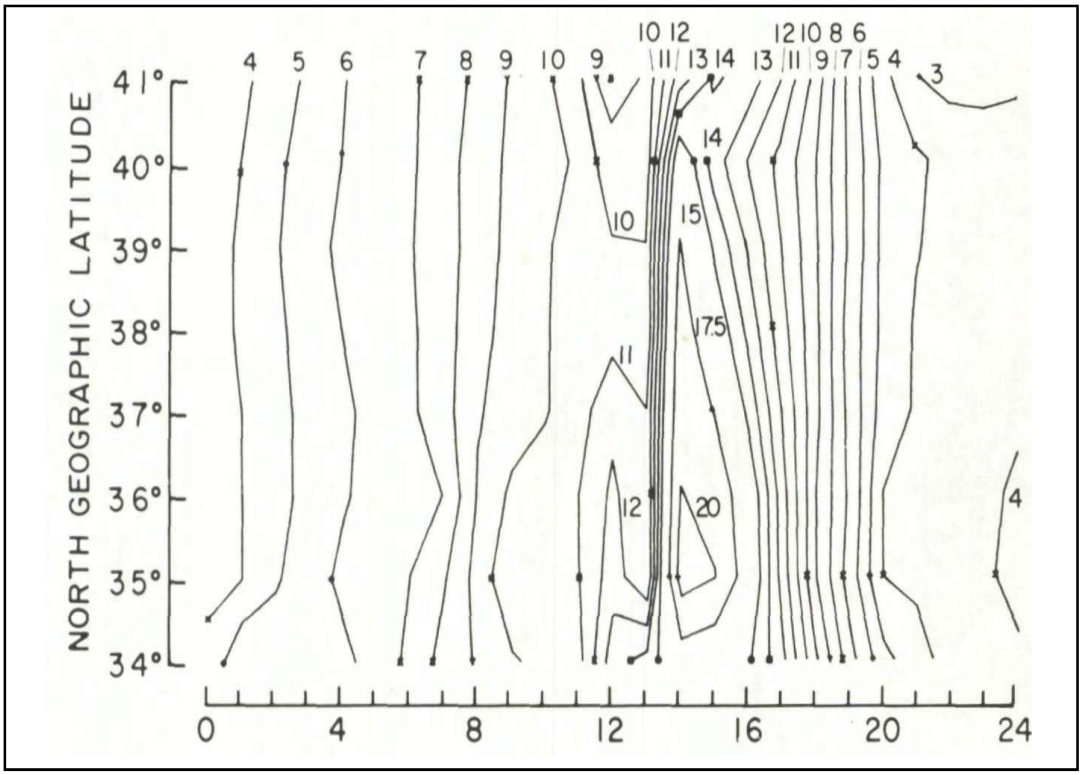

Figure 2. Contour plots of measured TEC data vs. hours and latitude for spring (TEC units are in10^{16} elektron/m^2)

The MLP_TEC network architecture is given in Figure 4 [11]. If the MLP processing function is provided with $\boldsymbol{y} = y(\boldsymbol{x}, W)$ where, $\boldsymbol{x}$ is the input vector, $\boldsymbol{y}$ is the output vector, and W is the total weight of the neural network [7-9], according to the equation (3) the input vector is $\boldsymbol{x} = [la, h]^T$, while the output output vector will be $\boldsymbol{y} = [TEC]$. The output of the l-th hidden layer of the MLP can be represented by the vector of the $\mathbf{y}_l$ dimension $N_l \times 1$ where N_l is the number of neurons in the l-th hidden layer, and where i-th element in that vector - $\mathbf{y}_l[i]$ represents the output i-th neuron of the s-th network layer ($s = l + 1$ also counting the input layer) $v_i^{(s)} = v_i^{(l+1)}$, i.e. stands $y_l = v_1^{(l+1)}, v_2^{(l+1)},..., v_{Ni}^{(l+1)}]^T$. That vector is

$$\mathbf{y}_l = F(\mathbf{w}_l \mathbf{y}_{l-1} + \mathbf{b}_l) \qquad (4)$$

where $\boldsymbol{y}_{l-1}$ is the dimension vector $N_{l-1} \times 1$ and represents the output of the (l-1)-th hidden layer, $\boldsymbol{w}_l$ is the matrix of the connection weight between the neurons of the (l-1)-th and l-th hidden layer dimensions $N_l \times N_{l-1}$, while $\boldsymbol{b}_l$ Represents the bias vector of the neuron of the l-th hidden layer.

In accordance with this notation, $\boldsymbol{y}_0$ represents the output of the input buffer layer, so that $\boldsymbol{y}_0 = \boldsymbol{x}$. Element $\mathbf{w}_l[i, j]$ weight matrix $\boldsymbol{w}_l$ Indicates the weight of the connection between the i-th neuron in the hidden layer (l-1) and j-th neuron in the hidden layer l, i.e. between i-th neuron in the network layer $s = l$ and j-th Neurons in the network layer $s = l$+1, while element $b_i^{(l)} = \boldsymbol{b}[i]$ Represents the bias value of the i-th neuron in the hidden layer l. Function F represents the activation function of neurons in hidden layers and in the case of MLP_TEC network it is a tanges hyperbolic sigmoidal function

$$F(u) = \frac{e^u - e^{-u}}{e^u + e^{-u}} \qquad (5)$$

All neurons from the last hidden layer H are connected with the neuron of the output layer. The activation function of the neuron in the last layer is linear, and the output of the MLP_TEC network is

$$TEC = \mathbf{w}_o \mathbf{y}_H \qquad (6)$$

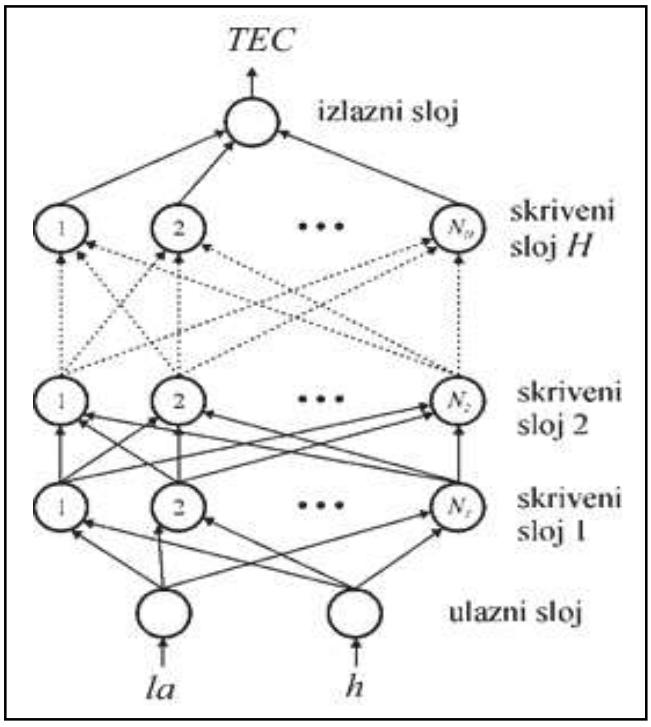

Figure 4. Architecture of the MLP_TEC neural network for TEC value estimation over the Mediterranean area [11]

where $\boldsymbol{w}_o$ is the the weight of the connection between the neuron of the H-th hidden layer and he neuron of the output layer with dimensions of $1 \times N_H$ (Figure 4). In line with this, the weight of the network looks like this: $W = \{\mathbf{w}_1,...,\mathbf{w}_H,\mathbf{w}_o,\mathbf{b}_1,...,\mathbf{b}_H\}$.

The general mark for this defined MLP neural model is MLPH-N_1-…-N_i-…-N_H where H Represents the total number of hidden layers of the MLP network used, while N_i represents the total number of neurons in the i-th hidden layer. Thus, the MLP2-12-10 designation, denotes a MLP model whose neural network has a total of four neural layers (input, output, and two hidden layers) and has 12 neurons in the first hidden layer and 10 neurons in the second hidden layer.

For realization and training of MLP_PA model MatLab development environment was used. The model was applied to determine the ionospheric carrier phase advance for the autumn and winter period. Training for different periods was carried out for both periods MLPH-N_1-…-N_i-…-N_H networks where stand $H = 2$ and $5 \leq N_i \leq 22$. In both cases, the Levenberg-Marquartd training method was used with a given training accuracy of 10-4. Each network was tested with an appropriate set of test samples to obtain its generalization characteristics expressed through the largest test error (WCE), the average test error (ATE), and the PPM correlation coefficient value (r^{PPM}) [7-11].

In the autumn period, the MLP_TEC network training and testing assemblies were obtained by reading the values from the graphics in Figure 1, at the cross-section points of the selected latitude and TEC range. In selecting the latitude value for the training set, a step of 1,,a in the range [34° 41°] so the training session had 250 samples. For the test set, a step of 2° in the range [35.5° 39.5°] was used, so the test set had 100 samples.

As for the spring period, using the same reading algorithm, but now in Fig. 2, training and test sets were obtained that had 233 and 90 samples respectively.

Table 1 and Table 2 show the test results for three MLP_TEC networks of autumn and winter periods respectively, which had the highest correlation coefficient value per test set. For the realization of the MLP_PA model in the autumn period, the network with the highest correlation coefficient was selected, which is MLP2-5-5 network. According to the same principle for MLP_PA model implementation in the spring period, MLP2-10-6 network was selected. In Fig. 5, a diagram of the dissipation of the MLP2-5-5 network on the test set of the autumn period is shown, while in Fig. 6, a diagram of the dissipation of the MLP2-10-6 network is displayed on the test set of the spring period.

MLP model	**WCE [%]**	**ACE [%]**	r^{PPM}
MLP2-5-5	15.27	2.87	0.9897
MLP2-6-6	14.68	3.26	0.9868
MLP2-10-5	15.42	3.23	0.9863

Table 1. Testing Results for Three MLP Models with the Highest R_{ppm} Value (Autumn)

MLP model	***WCE* [%]**	***ACE* [%]**	r^{PPM}
MLP2-10-6	16.14	2.87	0.9868
MLP2-5-5	15.58	2.99	0.9862
MLP2-6-6	15.82	3.16	0.9846

Table 2. Testing Results for Three MLP Models with the Highest R_{ppm} Value (Spring)

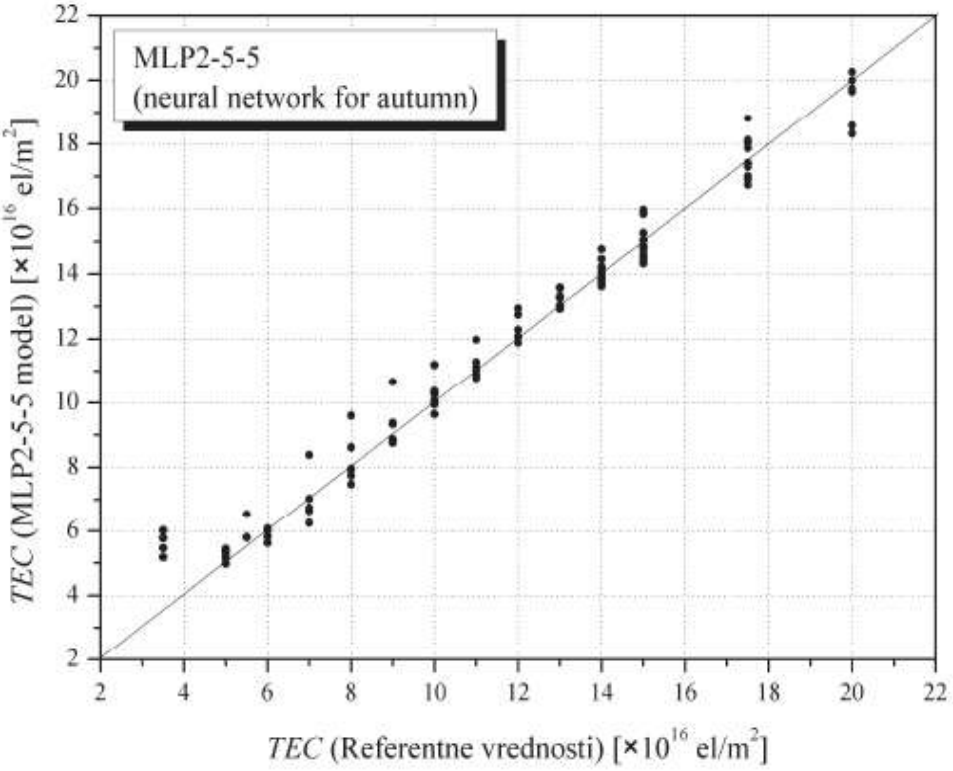

Figure 5. Scattering Diagram For Mlp2-5-5 Model (Autumn, Test Set)

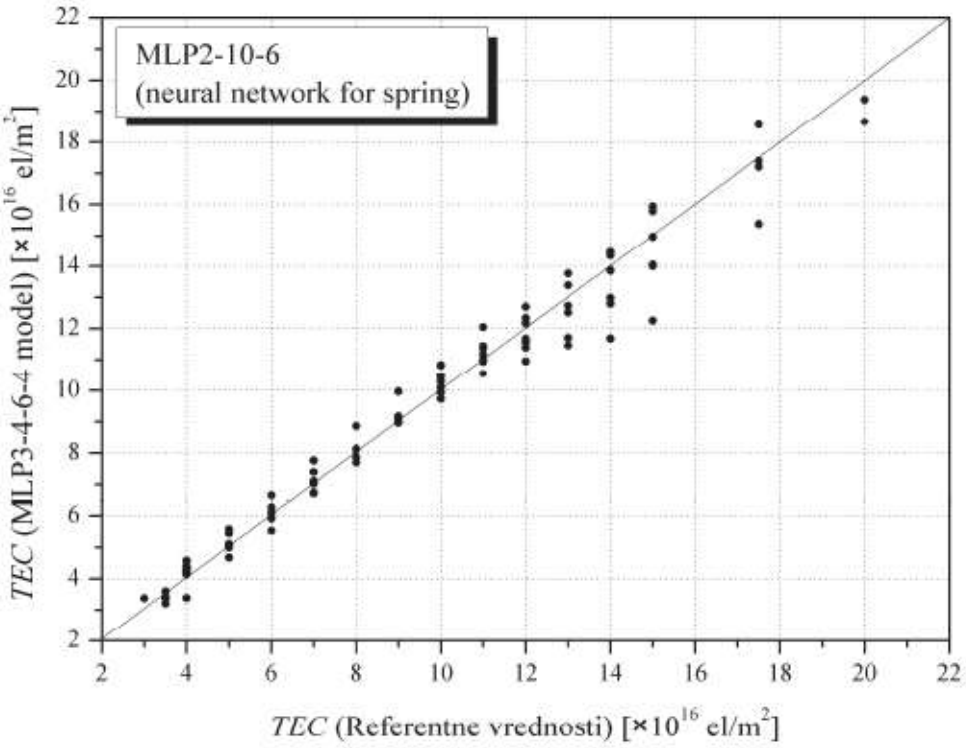

Figure 6. Scattering diagram for MLP2-10-6 model (spring, test set)

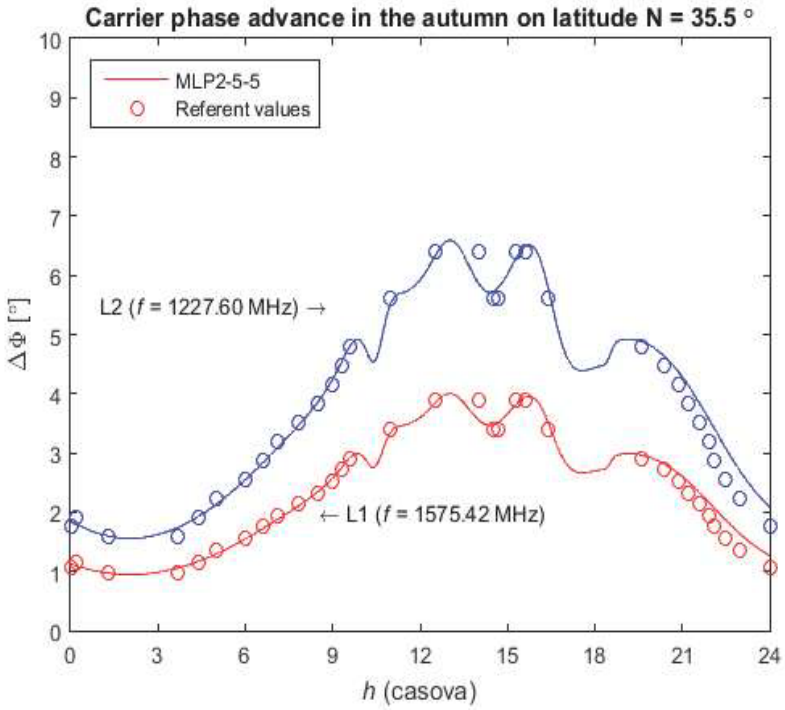

Figure 7. Ionospheric carrier phase advance of the GPS signal at L1 and L2 frequencies in 24 h autumn period for latitude *la* (N) = 35.5^0 obtained by $MLP\_PA_{(MLP2\text{-}5\text{-}5)}$ model

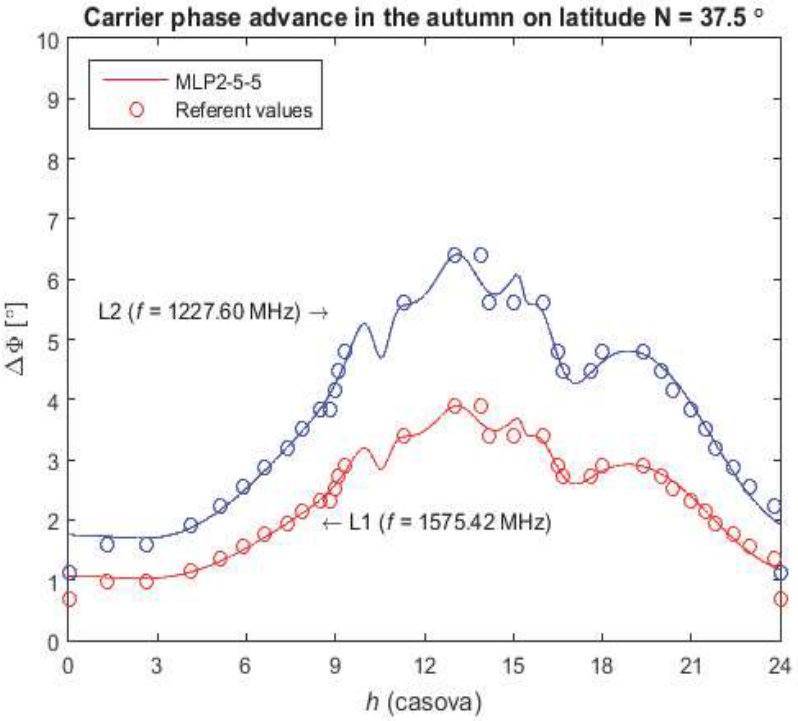

Figure 8. Ionospheric carrier phase advance of the GPS signal at L1 and L2 frequencies in 24 h autumn period for latitude *la* (N) = 7.5^0 obtained by $MLP\_PA_{(MLP2\text{-}5\text{-}5)}$ model

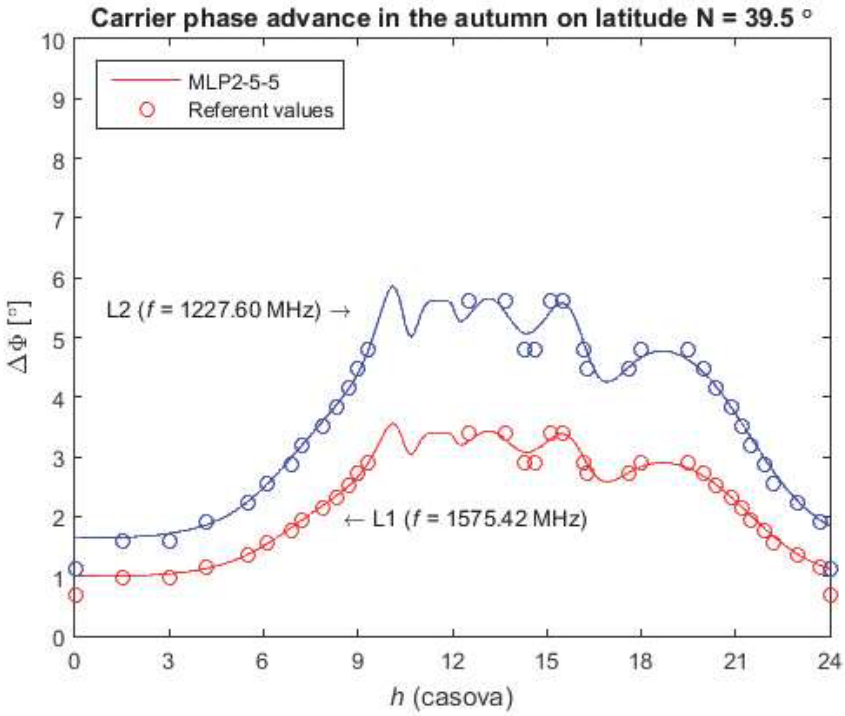

Figure 9. Ionospheric carrier phase advance of the GPS signal at L1 and L2 frequencies in 24 h autumn period for latitude *la* (N) = 39.5^0 obtained by $MLP\_PA_{(MLP2\text{-}5\text{-}5)}$ model

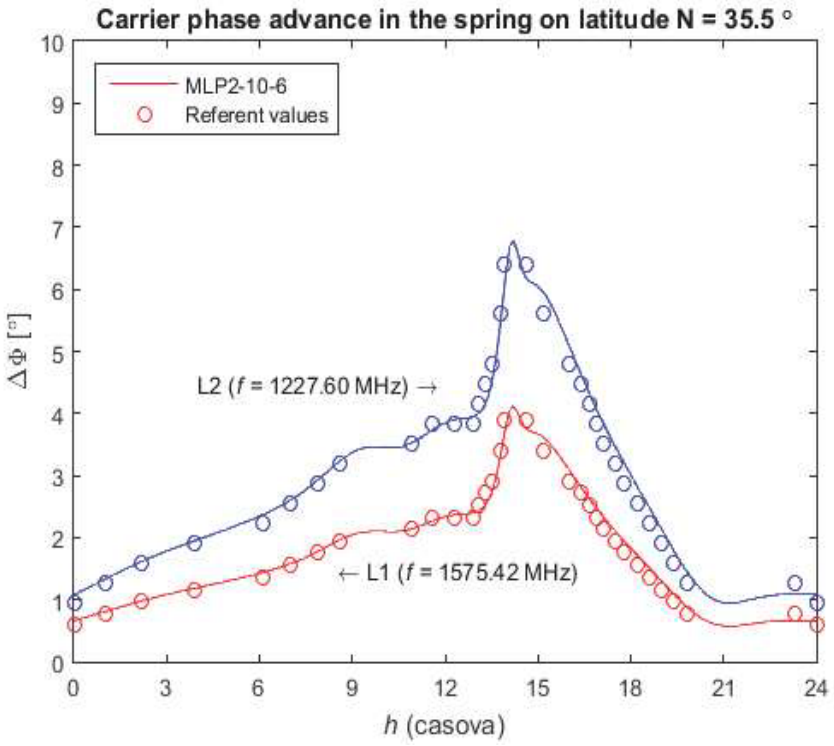

Figure 10. Ionospheric carrier phase advance of the GPS signal at L1 and L2 frequencies in 24 h spring period for latitude *la* (N) = 35.5^0 obtained by $MLP\_PA_{(MLP2\text{-}10\text{-}6)}$ model

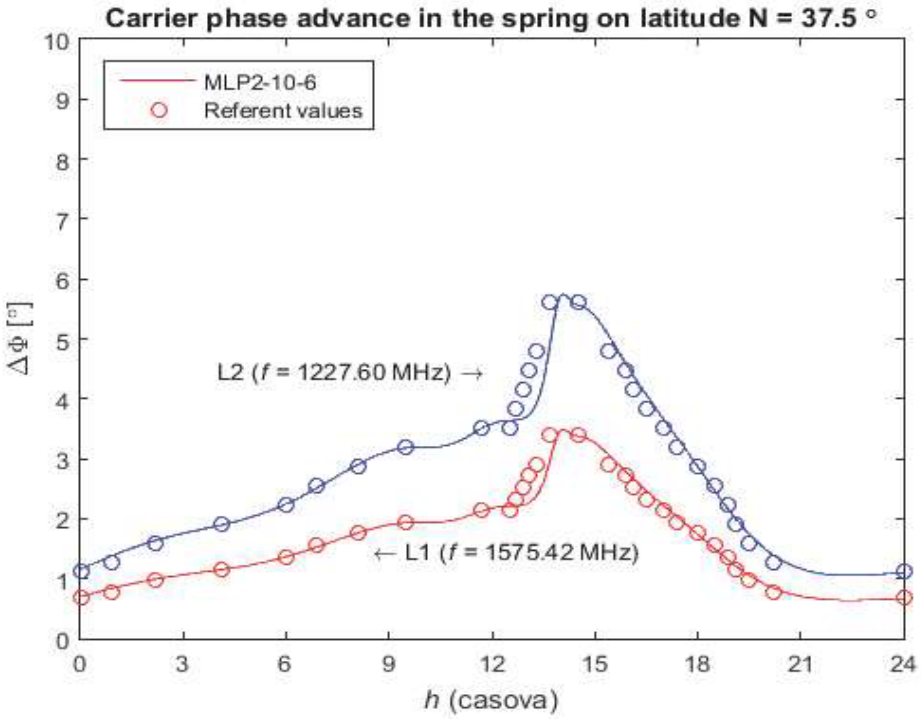

Figure 11. Ionospheric carrier phase advance of the GPS signal at L1 and L2 frequencies in 24 h spring period for latitude *la* (N) = 35.5^0 obtained by $MLP\_PA_{(MLP2\text{-}10\text{-}6)}$ model

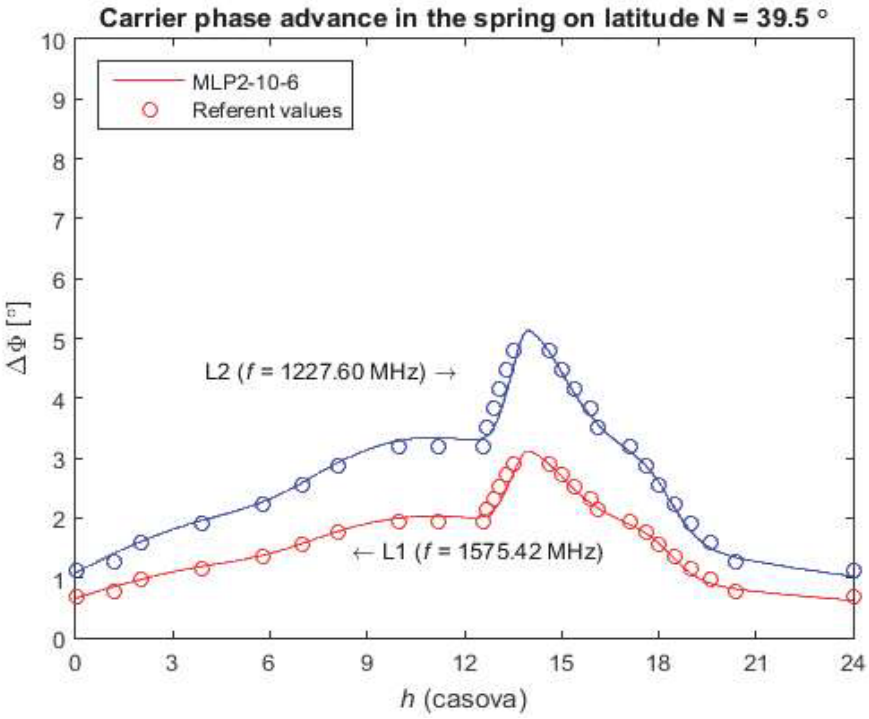

Figure 12. Ionospheric carrier phase advance of the GPS signal at L1 and L2 frequencies in 24 h spring period for latitude *la* (N) = 35.5^0 obtained by $MLP\_PA_{(MLP2\text{-}10\text{-}6)}$ model

The MLP_PA model for the autumn period was realized using the trained MLP2-5-5 network and bears the mark $MLP\_PA_{(MLP2-5-5)}$, The model for the spring period is labeled $MLP\_TD_{(MLP2-10-6)}$ because model MLP2-10-6 of the network was used for its realization. These models are used to simulate ionospheric carrier phase advance GPS of the systems on L1 and L2 frequencies (Figure 7-12).

.

Ionospheric carrier phase advance of the GPS signal at L1 and L2 frequencies in 24 h autumn period for latitude *la* (N) = 35.5^0, 37.5^0 and 39.5^0 obtained by $MLP\_PA_{(MLP2-5-5)}$ model are shown in the Figure 7, 8 and 9. respectively. For each longitude value, this model generated the ionospheric carrier phase advance values for a 6-minute daily period, which means at 241 points. Resaults obtained by the $MLP\_TD_{(MLP2-5-5)}$ model are compared with the reference values obtained by direct application of formula (1) to TEC values read from the graphics in Figure 1, it can be observed that good results are obtained by a neural model with reference values. Figures 10- 12 show the values of ionospheric carrier phase advance of the GPS signal at L1 and L2 frequencies in 24 h spring period for latitude *la* (*N*) = 35.5^0, 37.5^0 and 39.5^0 obtained by $MLP\_PA_{(MLP2-10-6)}$ model. Also, in this case, for each latitude, this model generates signal delay values for a daily period with a resolution of 6 min, which means at 241 points. The results obtained by the neural model were compared with the reference values obtained by reading from Figure 2. For the spring period, a good values can be made between the obtained results with the reference values.

4. Conclusion

To describe changes in the characteristics of EM waves that extend through the ionosphere, it is vital to determine the concentration of free electrons on the path of expansion through the ionosphere or TEC value. Today, for the determination of TEC values at the desired location, either complex numerical-empirical models for generating profile of the ionosphere are based on specialized software available to a narrow set of users (for example, scientific and military organizations of large countries) for geographical areas that meet their needs, Or empirical data obtained by measurementson a limited number of spatial-temporal locations around the world and which are organized through a large number of tables and graphics. Determining the TEC value by visual reading for the isocontact of the selected graphics and using manual interpolation can take a long time and can be imprecise. It is shown that the modeling of the dependence of TEC values shown in the graphs using multilayer perceptron networks can increase the speed and precision of the procedure for determining the TEC value, and therefore can automate the procedures for determining changes in the TEC dependent parameters of the EM signal when it passes through the ionosphere.

The presented results of the application of the MLP_PA neural model for determining the ionospheric carrier phase advance for the autumn and spring period of the Mediterranean region confirm the justification of the application of models based on artificial neural networks in the process of characterizing the EM signal extending through the ionosphere. The results also confirm that the neuronal model can be a good alternative to expensive and hardwarechallenging numerical models and software to describe the impact of the ionosphere on the EM wave propagation as well as slow and rough calculations based on manual use of TEC graphics.

Acknowledgement

This paper is supported by the project TR-32052 and TR- 32054 of the Ministry of Education in the Republic of Serbia.

References

[1] Dragovi, M. (1996). *Antene i prostiranje radio talasa*, Beopres, Beograd, 1996.

[2] Mitic, Maja. S. (2002). *Jonosfera*, Astronomski magazin, april, 2002., http://static.astronomija.co.rs/suncsist/planete/zemlja/jonosfera/jonosfera.htm.

[3] Stevanovi, Ž. (2010). *Radio-amaterske analogne KT i UKT komunikacije u Srbiji*, Radioamater br. 2., 2010.

[4] Pratt, T., Bostian, C.W., Allnutt, J. E. (2003). *Satellite Communications*, John Wiley and Sons, 2003. god.

[5] Basu, S., Buchau, J., Rich, F. J., Weber, E. J., Field, E. C., Heckscher, J. L., Kossey, P.A. E.A. Lewis, B.S. Dandekar, L.F. McNamara, E.W. Cliver, G.H. Millman, J. Aarons, S. Basu, J.A. Klobuchar, S. Basu, M.F. Mendillo, *Ionospheric Radio Wave Propagation, Chapter 10*, http://www.ngdc.noaa.gov/stp/spaceweather/online-publications/miscellaneous/afrl_publications/handbook_1985/Chptr10.pdf

[6] Klobuchar, J.A., Aarons, J. (1973). Numerical Models of Total Electron Content Over Europe and the Mediterranean and Multi-station Scintillation Comparisons, INTERNATIONAL AGARD Agardograph,1973.

[7] Haykin, S. (1994). *Neural Networks*, New York, IEEE, 1994.

[8] Zhang, Q. J., Gupta, K. C. (2000). *Neural Networks for RF and Microwave Design*, Artech House, 2000.

[9] Christodoulou, C., Georgiopoulos, M. (2001). *Applications of Neural Networks in Electromagnetics*, Artech House, 2001.

[10] Milovanovi, I., Stankovi, Z., Agatonovi, M., Miliji, M. (2012). Efficient Neural Model for Estimation of the Microwave Antenna Noise Temperature, *ICEST* 2013 *Conference*, Ohrid, Macedonia, June 26–29, 2012, pp. 425-428.

[11] Stankovi, Z., Milovanovi, I., Jovanovi, J., Don ov, N., Milovanovi, B. (2017). Estimation of the EM Wave Propagation Delay in the Ionosphere using Artificial Neural Networks, *YUINFO* 2017 *Conference*, March 12-15, Kopaonik, Serbia.